Pergamon

Electrochimica Acta, Vol. 43, Nos. 1–2, pp. 3–12, 1998

Printed in Great Britain

PII: S0013-4686(97)00222-3

0013-4686/98 $19.00 + 0.00

Sequential *in situ* STM imaging of electrodissolving copper in different aqueous acid solutions

M. E. Vela, G. Andreasen, S. G. Aziz*, R. C. Salvarezza and A. J. Arvia†

Instituto de Investigaciones Fisocoquímicas Teóricas y Aplicadas (INIFTA), Sucursal 4, Casilla de Correo 16, (1900) La Plata, Argentina

(Received 16 October 1996; accepted 17 February 1997)

Abstract—The dynamics of Cu surfaces immersed in either aqueous $HClO_4$ or H_2SO_4 solution under galvanostatic conditions at room temperature was studied by *in situ* scanning tunneling microscopy (STM) sequential imaging. The mobile interface depends considerably on the apparent current density (j) applied to the specimen. At $j = 0$, the Cu topography turns out to be highly dynamic as mass transport among different domains takes place. Conversely, for $j = 6\ \mu A\ cm^{-2}$ an inhomogeneous attack of the Cu surface leading to a remarkable increase in roughness and to the formation of etched pits at certain surface domains can be observed. Etched pit domains drive the mobile interface to an unstable regime. The addition of HCl to those acid solutions to reach concentrations higher than 10^{-2} M leads to the formation of a Cu_2Cl_2 layer. © 1997 Elsevier Science Ltd.

1. INTRODUCTION

In general, the study of the morphology of mobile interfaces produced in those processes involving the removal of material from solid surfaces becomes particularly relevant as it provides information about a number of processes at the local level which are usually beyond the possibility of being distinguished from global kinetic studies.

In recent years, the interest on the dynamics of anodic dissolution of different materials is rapidly increasing [1–7], as this approach to electrochemical kinetics indicates intricate process mechanisms. In this respect, a few theoretical models have been advanced [8–12], and experimental data concerning the evolution of some metal/aqueous solution interfaces have been reported [13, 14].

It has been shown that the dissolving interface under conditions far from equilibrium leads to the appearance of an irregular topography whose shape and evolution result from a competition among different physical processes [15–18]. From the temporal and spatial analysis of surface profiles based upon a relative simple framework [18], it has been concluded that a self-affine fractal surface which reaches a steady state roughness regime should be expected when the interface growth is dominated by either a simple or complex surface process, whereas an irregular profile under an unstable interface regime should be produced when those surface processes are coupled with either an electrical or a concentraton field built up around the mobile interface [17].

Most of the previous work on the kinetics and mechanism of solid metal attack by aggressive aqueous environments has been particularly focused from the standpoint of classical electrochemical kinetics [19, 20]. It has been concluded that commonly, at a low dissolution rate, the kinetics of the reaction is dominated by surface processes involving mainly an interfacial charge transfer at surface sites where metal atoms in the lattice are more weakly bound. The number of such active sites depends on the crystallographic structure and the topography of the metal surface. On the other hand, at a high dissolution rate, metal electrodissolution is controlled by a Laplacian field either uniformly or non-uniformly established around the corroding specimen.

*Visiting Professor from the Department of Chemistry, University of King Abdulaziz, Jeddah, Saudi Arabia
†Author to whom correspondence should be addressed.

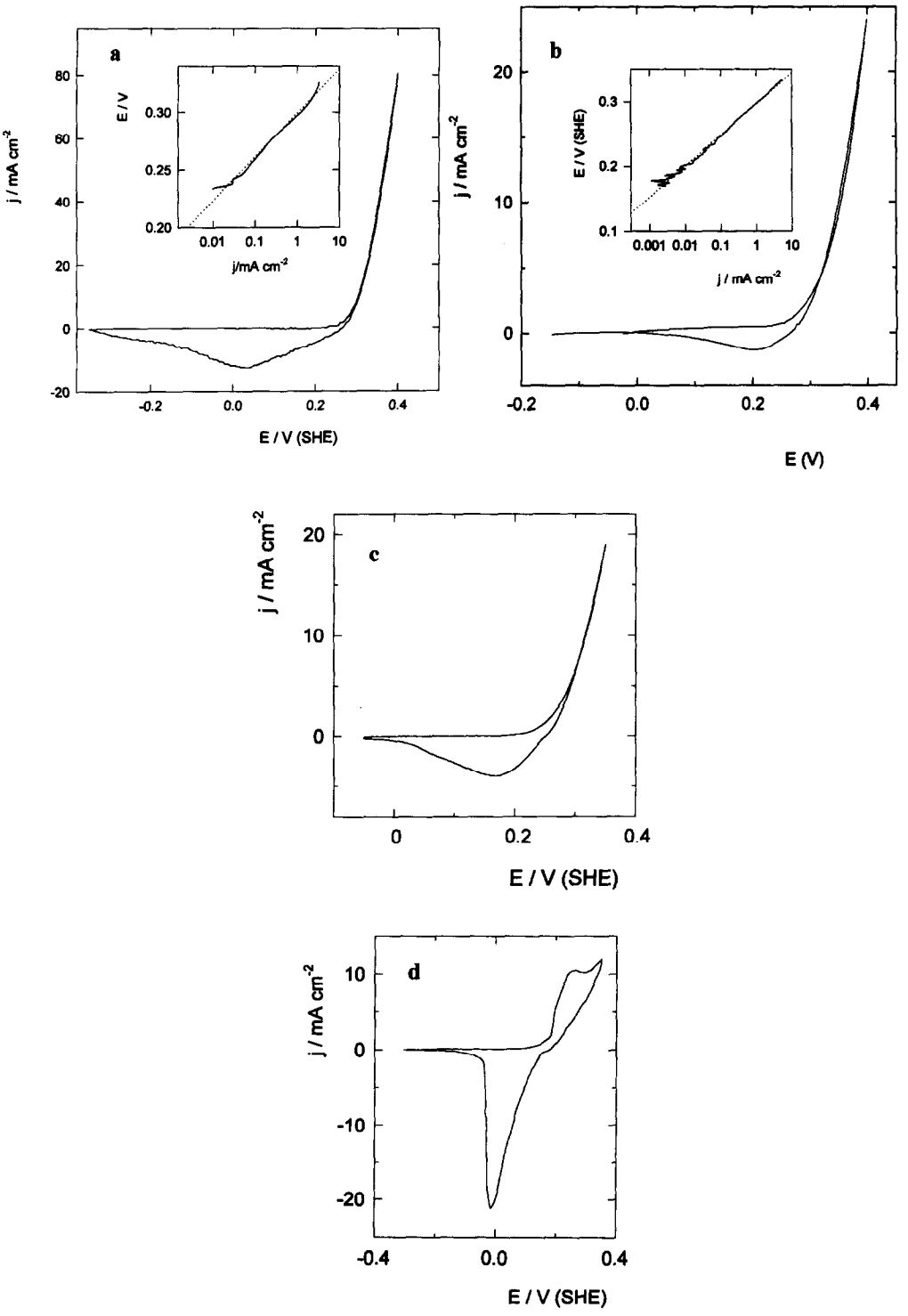

Fig. 1. Voltammograms of a Cu electrode recorded at 0.05 V s^{-1}. T = 298 K. (a) aqueous 0.5 M H_2SO_4. E vs log j plot obtained at 0.001 V/s is also shown. (b) aqueous 1 M $HClO_4$. E vs log j plot obtained at 0.001 V/s is also shown. (c) aqueous 1 M $HClO_4$ + 10^{-3} M HCl. (d) aqueous 1 M $HClO_4$ + 10^{-2} M HCl.

In contrast to surface crystallography (nm level), surface topography (10–100 nm level) has not been specifically considered in most theories of metal electrodissolution in aggressive media. In fact, the kinetic description of these processes has been usually based upon average kinetic parameters in the relationships between the reaction rate and the activation energy. However, due to the stochastic nature of the dynamics of metal dissolution, the surface topography (mobile interface) changes with

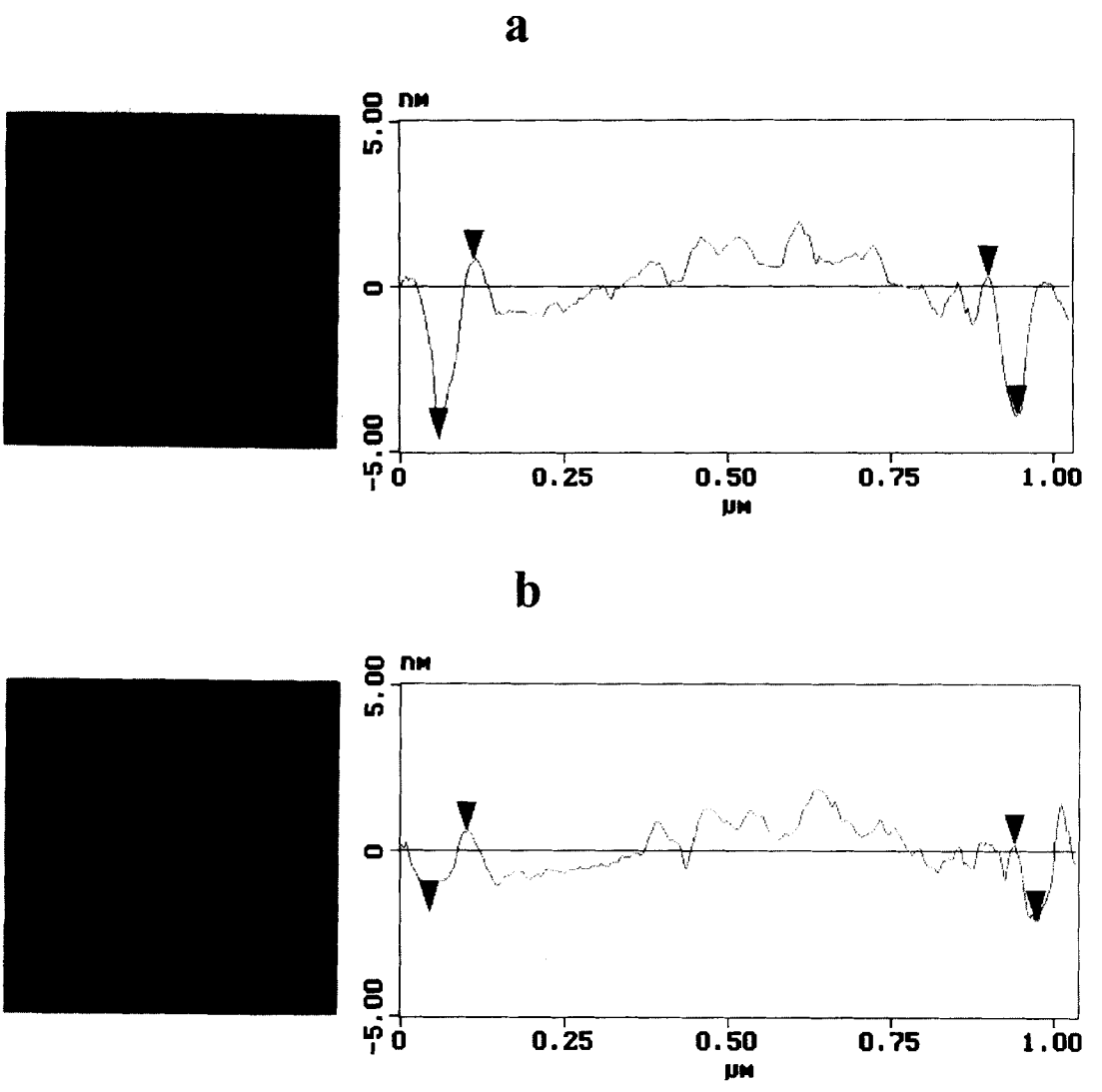

Fig. 2. *In situ* STM images (top view, $1000 \times 1000\ nm^2$ and section analysis of Cu surfaces for $j = 0$; aqueous 1 M $HClO_4$; $T = 298$ K. (a) Initial topography. (b) Topography after a 767 s immersion time.

time, in many cases evolving from a smooth to an irregular topography. Then, it should be expected that the topography of the corroding metal will reflect in some cases the kinetics and mechanism of the overall process [21].

Recently, the interface evolution for the electrodissolution of Ag crystal surfaces in contact with aqueous 1 M $HClO_4$ under the regime of a surface reaction control has been studied by *in situ* sequential STM imaging [13]. Accordingly, at low current density ($j < 15\ \mu A\ cm^{-2}$), the process approaches a layer by layer dissolution mechanism without a significant surface roughening, whereas for a high electrodissolution rate ($j > 15\ \mu A\ cm^{-2}$) a rough interface is produced. Then, the characteristics of the mobile interface result from a competition between void formation and smoothing processes.

This work describes the mobile interface of Cu domains in contact with either aqueous 1 M $HClO_4$ or aqueous 0.5 M H_2SO_4 under galvanostatic condition, resulting from *in situ* STM sequential imaging. For this purpose, the potential was restricted to a range in which Cu electrodissolution is under surface reaction kinetic control. For both acid solutions, under the condition $j = 0$, the growth of certain domains and the smoothing of small pits initially present in the surface can be observed. Conversely, for $j = 6\ \mu A\ cm^{-2}$, Cu electrodissolution proceeds inhomogeneously, that is, while some surface domains become rougher, others develop etched pits which drive the mobile interface to an unstable regime. Otherwise, when a concentration of HCl higher than 10^{-2} M is added to those acid solutions the electroformation of a $Cu_2\ Cl_2$ layer on the Cu surface is detected.

2. EXPERIMENTAL

The electrodissolution of Cu specimens was performed in the electrochemical setup provided with

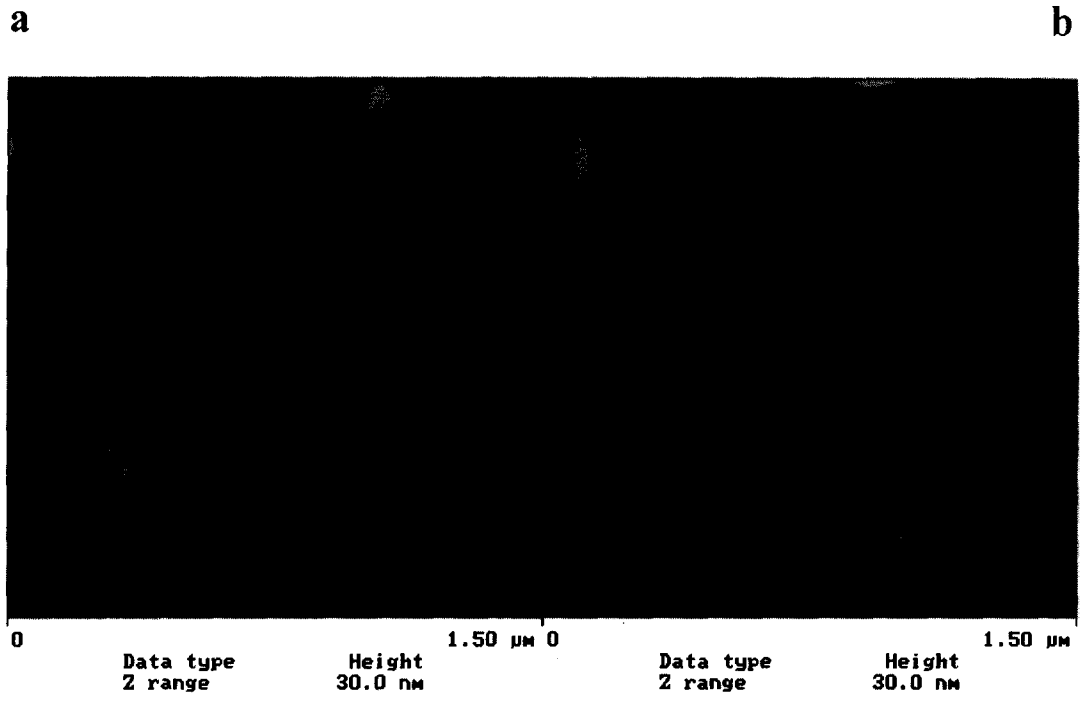

Fig. 3. *In situ* STM images (top view, $1500 \times 1500\ nm^2$) of Cu surfaces taking $j = 0$ in aqueous 0.5 M H_2SO_4. (a) Initial topography. (b) Topography after a 2 h immersion time.

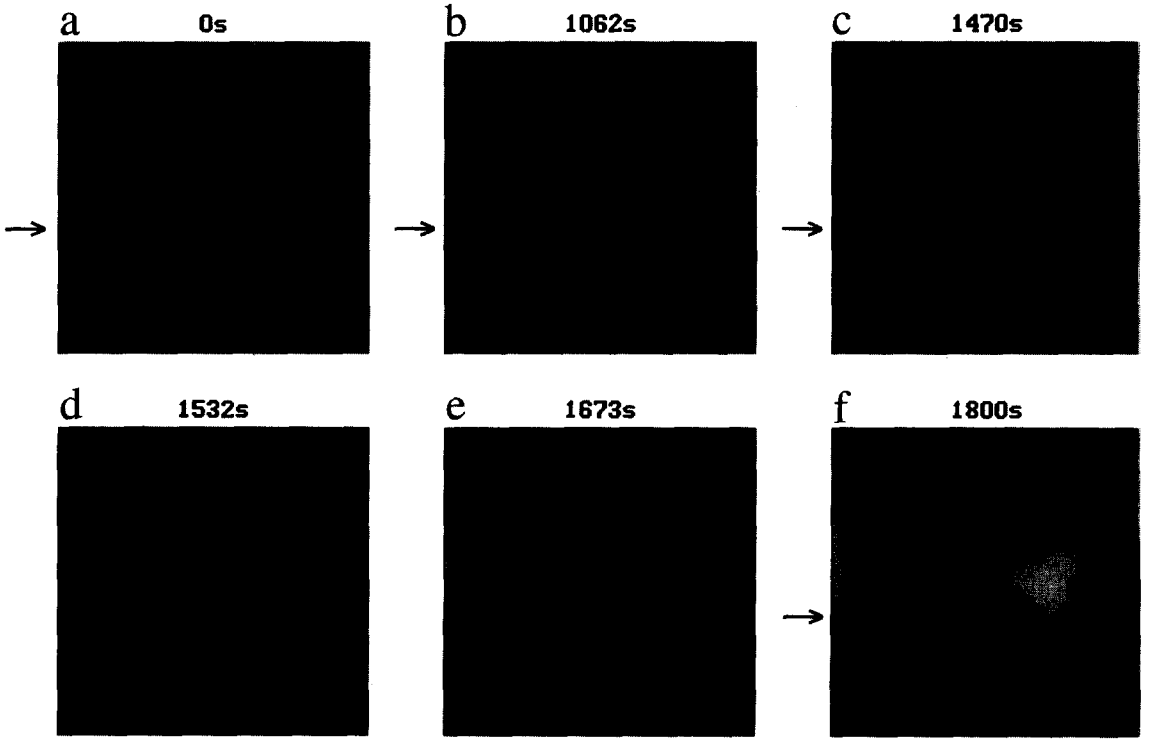

Fig. 4. Sequential *in situ* STM images (top view, $1500 \times 1500\ nm^2$) for Cu electrodissolution in aqueous 0.5 M H_2SO_4 for $j = 6\ \mu A\ cm^{-2}$. The electrodissolution time is indicated in the upper part of each picture. The image shown for 0 s was taken immediately after j was stepped from 0 to 6 μA. $T = 298$ K. Arrows indicate the sites where the cross-sections shown in Fig. 5(a) were determined.

the Nanoscope III STM (Digital Instruments, Santa Barbara CA) equipment, which consisted of a small Kel-F cell ($1.1 \times 2.0\ cm^2$ in size) provided with a polycrystalline Cu plate (99.99% purity) working electrode (exposed area $0.5\ cm^2$), a Pt counter electrode, and a $Pd/H_2/H^+$ reference electrode. Each working electrode was first mechanically polished, and then annealed at 400°C under a H_2 atmosphere resulting in a Cu surface formed by smooth terraces and steps only a few atoms in height and a relatively low density of surface defects. The SEM-EDX spectra of working electrode surfaces exhibited only the Cu signal when randomly selected regions of the Cu foil were scanned. The STM images of Cu specimens showed μm-sized ordered terrace domains with well-defined steps. These features made it possible to select smooth crystal domains $2000 \times 2000\ nm^2$ in size whose topographic changes could be followed by sequential *in situ* STM imaging.

Runs were made at $T = 298$ K in aqueous 1 M $HClO_4$ and aqueous 0.5 M H_2SO_4. Occasionally, aqueous HCl solution was added to those acid solutions to reach a HCl concentration in the range $10^{-3}\ M \leq c_{HCl} \leq 10^{-2}\ M$. Solutions were prepared from either 70% $HClO_4$ (Merck, p.a.) or 98% H_2SO_4 (Merck p.a.) and Milli-Q* water, and kept under purified N_2. Both the electrochemical cell and the STM head were placed in a properly shielded glass chamber under a continuous flow of purified N_2.

Conventional voltammograms of Cu immersed in the different solutions were recorded at two potential sweep rates, namely, $v = 10^{-3}\ V\ s^{-1}$ and $v = 5 \times 10^{-2}\ V\ s^{-1}$, covering the potential range −0.35 V to 0.40 V. From these runs the most convenient potential window for the *in situ* STM imaging of Cu specimens was selected. All potentials in the text are referred to the standard hydrogen electrode (*she*) scale.

Sequential *in situ* STM imaging was made in the following way. First, the Cu electrode was polarized at $E = -0.05$ V, *ie* a potential at which no Cu electrodissolution was observed. Then, after drift attenuation, a series of STM images of a smooth surface domain, typically $2000 \times 2000\ nm^2$, were taken for 20 min at $j = 0$ to check the stability of the Cu electrode topography. Under these circumstances the root mean square roughness of the surface ($\langle \xi_{STM} \rangle$) was 1 nm or thereabouts. Later, by setting $j > 0$, the sequential *in situ* STM imaging of the Cu surface was pictured at typically from a 1 to 3-min interval up to $t = 5000$ s. To obtain quantitative information about Cu electrodissolution thirty STM images at least for each specimen were analyzed.

STM imaging was made using Pt–Ir Nanotips covered by Apiezon wax to minimize the possible interference of faradaic currents.The following conditions for *in situ* STM imaging were used: tip potential in the range $0.10\ V \leq E_t \leq 0.35\ V$; tunneling current $I_t = 2$ nA; bias voltage $E_b = 0.1$ V, and scanning rate 5 Hz. The value of E_t was always in the double layer potential range of the tip material in the solution, and it was chosen sufficiently positive to avoid electrodeposition on the tip of dissolving Cu from the substrate. STM data were analyzed after instrument plane removal, as described elsewhere [22, 23].

Occasionally, *ex situ* scanning force microscopy (SFM) imaging of Cu topography was also made to discard the presence of tip induced artifacts during the *in situ* STM imaging. These runs were made using a Nanoscope III AFM equiment (Digital Instruments, Santa Barbara, CA) operating in the contact mode. Au cantilevers with integral Si_3N_4 tips were used. Typical forces used in these experiments were 10 nN.

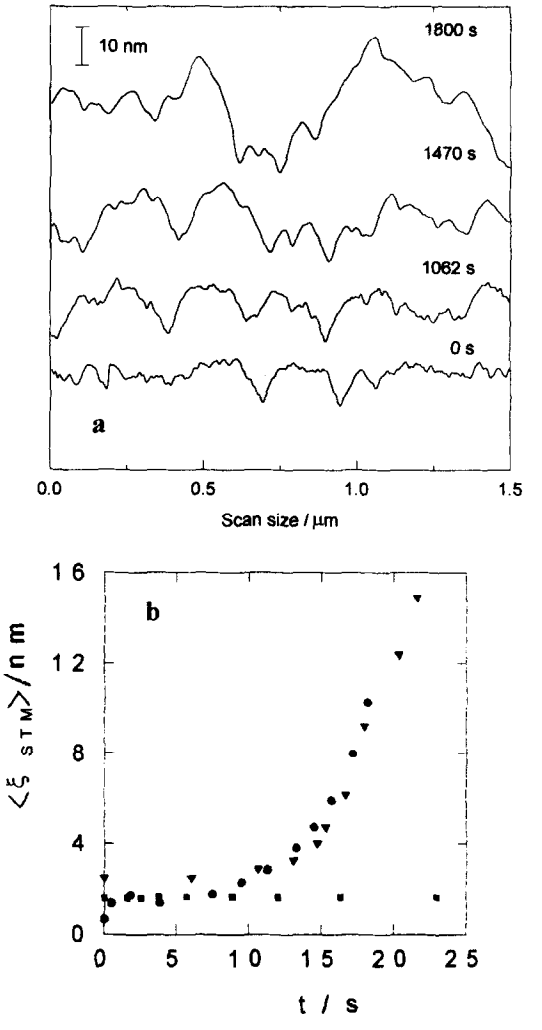

Fig. 5. (a) STM scans obtained at different Cu electrodissolution times in aqueous 0.5 M H_2SO_4. (b) (ξ_{STM}) vs t plots derived from STM imaging for $j = 6\ \mu A\ cm^{-2}$ in (▼) aqueous 0.5 M H_2SO_4, (●) aqueous 1 M $HClO_4$, (■) aqueous 1 M $HClO_4$ + 10^{-2} M HCl.

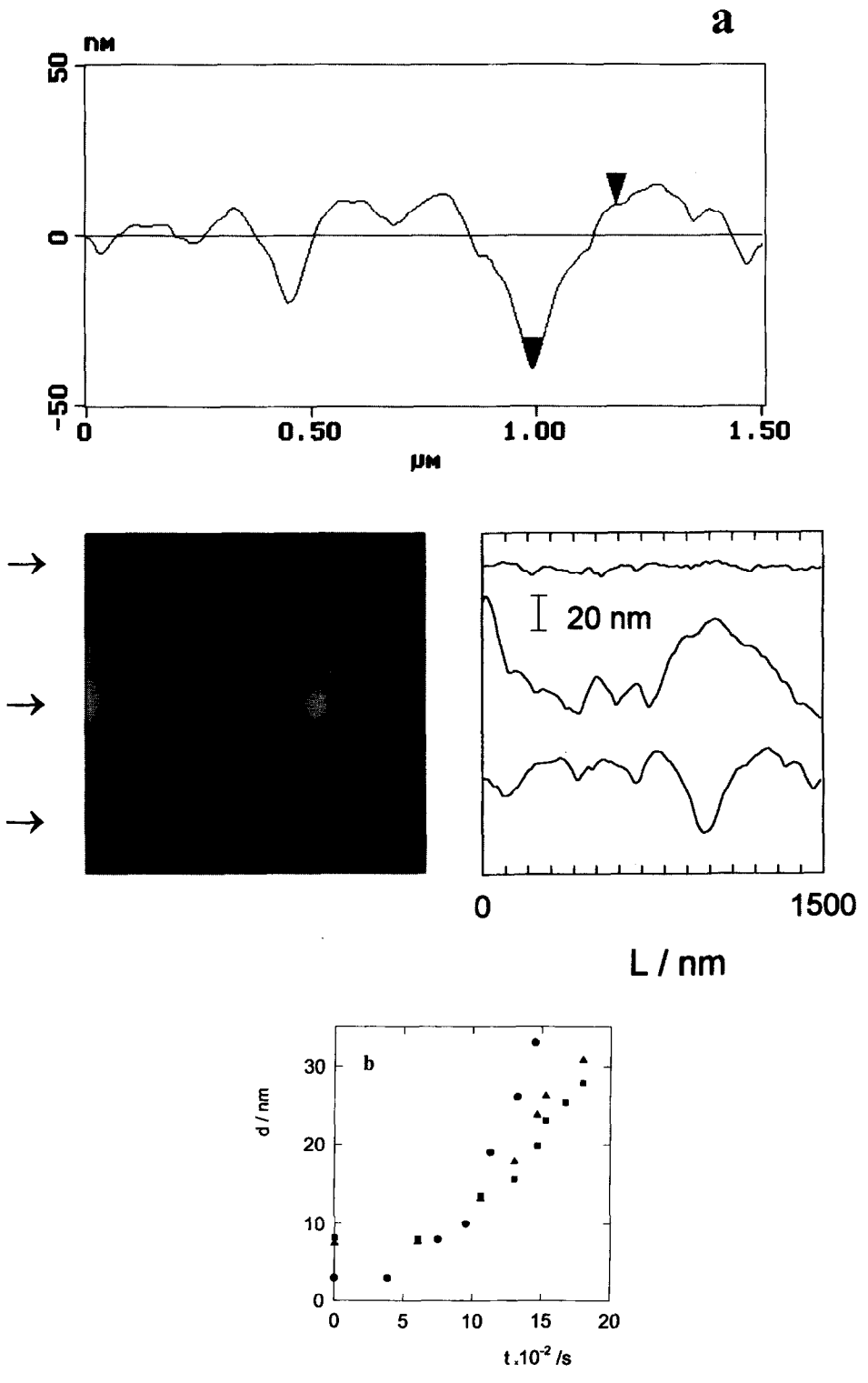

Fig. 6. (a) STM section analysis for pit depth evaluation. Right hand side. Typical STM cross sections at different domains showing roughening and pitting of the Cu surface. (b) d vs t plots for pits grown in (▲, ■) aqueous 0.5 M H_2SO_4 (j = 6 μA cm^{-2}), (●) aqueous 1 M $HClO_4$ (j = 6 μA cm^{-2}). Average rate of etched pit penetration ≅0.2 atom s^{-1}.

3. RESULTS AND DISCUSSION

3.1 Electrochemical data

The voltammogram for polycrystalline Cu in aqueous 0.5 M H_2SO_4 run at $v = 0.05\ V\ s^{-1}$ from -0.28 V to 0.40 V (Fig. 1(a)) shows a null current from -0.28 V to 0.20 V followed by a rather fast anodic current increase when the Cu electrodissolution threshold potential is reached. Subsequently, the reverse potential scan exhibits a broad cathodic current peak at $E = 0.20$ V which is related to the electroreduction of soluble Cu species produced in the preceding scan.

The log j vs E plot resulting from anodic polarization at $v = 10^{-3}\ V\ s^{-1}$ for $E > 0.25$ V yields a reasonable straight line with a slope $b_a \cong 0.040$ V decade^{-1} (Fig. 1(a), inset), in agreement with data already reported in the literature [24]. Similar results are obtained in aqueous 1 M $HClO_4$ (Fig. 1(b)).

The voltammogram of Cu specimens in aqueous 1 M $HClO_4$ + HCl ($c_{HCl} \leq 10^{-3}$ M) (Fig. 1(c)) is very similar to those obtained in the absence of HCl. However, drastic voltammetric changes can be observed in 1 M $HClO_4$ + HCl ($c_{HCl} \geq 10^{-2}$ M) (Fig. 1(d)), as in this case a rather complex anodic

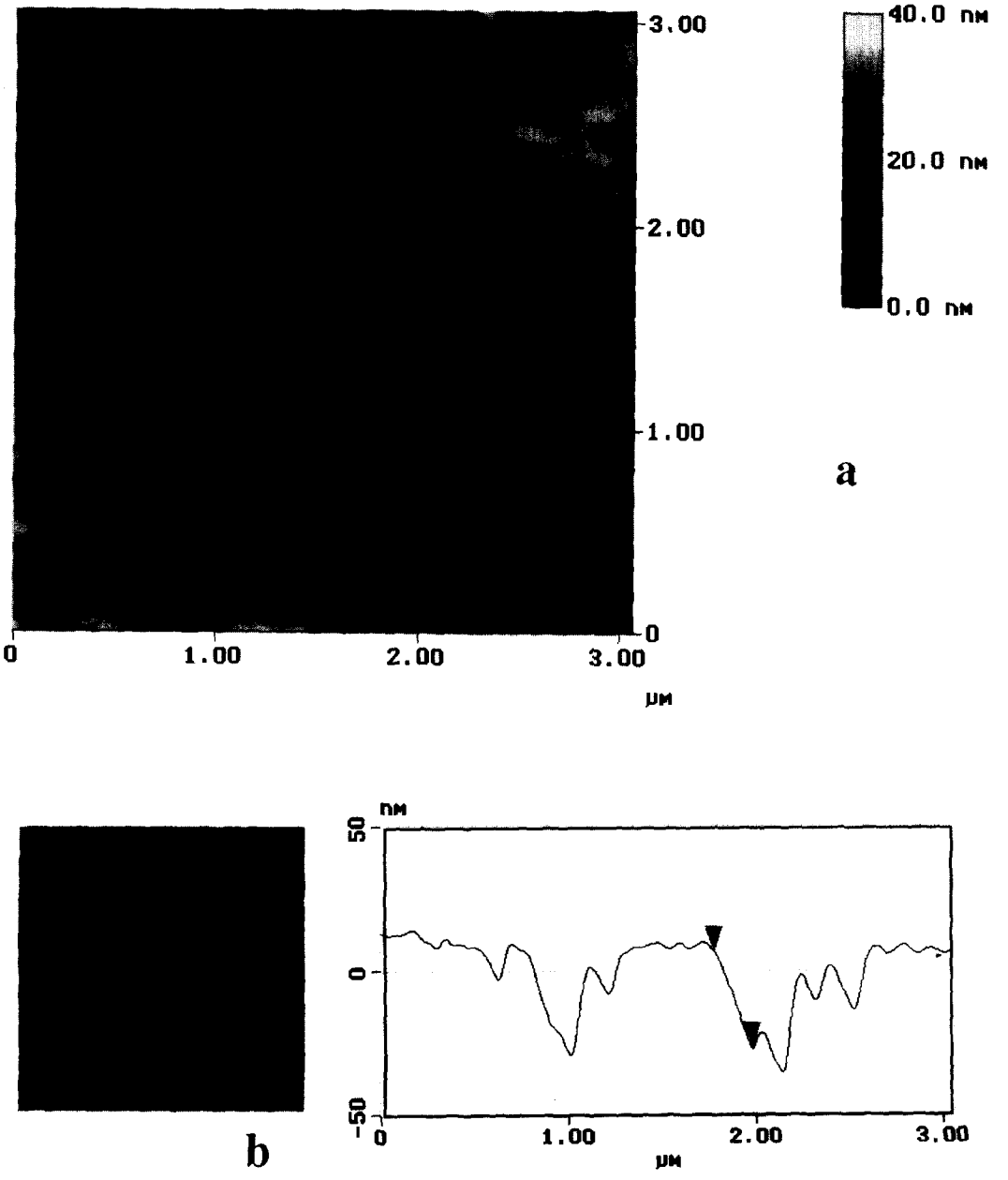

Fig. 7. (a) *Ex situ* SFM images (3000 × 3000 nm^2) of a Cu specimen after 30 min immersion in aqueous 1 M $HClO_4$ at $j = 6\ \mu A\ cm^{-2}$. (b) Section analysis of pits shown on (a).

current peak at *ca.* 0.22 V, and a large asymmetric cathodic peak at *ca.* 0 V can be observed in the reverse scan. These peaks are related to the electroformation and eletroreduction of a Cu_2Cl_2 layer on Cu [25].

3.2 Sequential *in situ* STM imaging

In situ STM images (topographic mode, $1000 \times 1000\ nm^2$) of a Cu crystal domain taken immediately after immersion in aqueous 1 M $HClO_4$ at $j = 0$ (Fig. 2(a)) show terraces with a number of homogeneously distributed bumps 1 to 2 nm in height (h), and a few small rounded pits 70 to 100 nm in radius (r) and about 5 nm in depth (d_s). Section analysis of the same domain (Fig. 2 (b)) reveals a decrease in d_s and a less noticeable decrease in r for small rounded pits.

The rate of pit filling estimated from the time dependence of d_s was *ca.* 0.003 nm/s. Assuming that the small pit filling is a surface diffusional controlled process, the average surface diffusion coefficient of species contributing to pit filling can be estimated from the relationship [26],

$$\Delta r^2 = 2Dt_f, \tag{1}$$

where t_f is the time required for filling a substrate monolayer, Δr is the decrease in the radius of the pit defined as

$$\Delta r = r(t_f) - r(t_{f=0}), \tag{2}$$

and D is the average surface diffusion coefficient of species filling the small pits. Data from our work in aqueous 1 M $HClO_4$ at $E = -0.05$ V result in $D \cong 10^{-15}\ cm^2\ s^{-1}$. It should be noted that the time scale involved in the smoothing process allowed us to discard that pit filling proceeded by a dissolution–deposition mechanism operating on the solution side. For such a case shorter times should be involved as the Cu^{2+} ion diffusion coefficient in aqueous solution is $D \cong 10^{-5}\ cm^2\ s^{-1}$ [27].

The dynamics of Cu surface in aqueous 0.5 M H_2SO_4 can also be confirmed by STM imaging for 2 h of a $1500 \times 1500\ nm^2$ domain (Fig. 3(a), (b)) which shows bumps and irregular cavities. For $j = 0$, a gradual change in the shape and orientation of bumps and their increase in size as well as the size of irregular cavities between the bumps can be observed. Accordingly, a slight increase in the root mean square roughness of global topography from $\langle \xi_{STM} \rangle = 2.0$ nm to $\langle \xi_{STM} \rangle = 2.3$ nm occurs due to bump coalescence and growth (Fig. 3(a), (b)). Therefore, from STM images it can be concluded that for $j = 0$, the topography of Cu in both acids is highly mobile.

In situ sequential STM images of Cu dissolving at $j = 6\ \mu A\ cm^{-2}$ in the same acids (Fig. 4(a)–(f)) show the progressive development of an irregular topography. This is clearly seen from both the section analysis of STM scans at different t (Fig. 5(a)), and the time dependence of $\langle \xi_{STM} \rangle$ (Fig. 5(b)). It should be noted that in this case, while certain Cu surface domains become noisy due to random electrodissolution (Fig. 6(a), upper part) others develop deep etched pits which turn the mobile interface unstable (Fig. 6(a), middle and bottom).

The etched pit growth kinetics for Cu immersed in either aqueous 1 M $HClO_4$ or 0.5 M H_2SO_4 can be determined from the section analysis of STM scans in a particular surface direction (Fig. 6(a)). In this case, after an induction time $t_1 \cong 1000$ s, the value if d increases almost linearly with t (Fig. 6(b)). From the slope of the linear portion of the d vs t plot for aqueous 0.5 M H_2SO_4, the average rate of etch pit penetration with respect to the outer electrode surface can be estimated as 0.2 atom s^{-1}. This penetration rate is almost 15 times greater than that calculated from Faraday's law considering the average current density over the entire electrode surface. After assuming a conical pit geometry and estimating an average etched pit surface area from STM images and section analysis, the average current density at pits $j_p \cong 0.1\ mA\ cm^{-2}$.

Similar results are obtained from Cu specimens immersed in aqueous 1 M $HClO_4$. Seemingly, ClO_4^- and HSO_4^- / SO_4^{2-} anions behave in a rather similar way for the evolution of Cu topography.

The fact that saturation is reached neither in the $\langle \xi_{STM} \rangle$ vs t plot (Fig. 5(b)) nor in the d vs t plot (Fig. 6 (b)) is a clear indication that the mobile interface of corroding Cu becomes unstable [17]. Therefore, it is reasonable to conclude that in both acids the unstable mobile interface regime is largely caused by the appearance of etched pits. Conversely, for Cu immersed in 1 M $HClO_4 + 10^{-2}$ HCl, the value of $\langle \xi_{STM} \rangle$ derived from *in situ* STM imaging remains practically constant with time (Fig. 5(b)), suggesting that Cu dissolution proceeds mainly through a layer by layer mechanism [28]. In fact, this explanation would agree with the mechanism involving Cu electrodissolution from the step edges which has been reported for Cu in the presence of Cl^- anions [28].

To exclude the possibility that the formation of etched pits under *in situ* STM imaging could be assigned to a tip-induced artifact, Cu electrodes were anodized for 30 min at $j = 6\ \mu A\ cm^{-2}$ in a conventional electrochemical cell containing aqueous 1 M $HClO_4$, and subsequently, the topography of the electrode was imaged by *ex situ* SFM. These images (Fig. 7) show crystallographic triangular-shaped etched pits formed on terraces (Fig. 7(a)). In this case, the section analysis (Fig. 7(b)) confirmed the value for the rate of etched pit reported above. Consequently, a tip-induced artifact during *in situ* STM imaging should be discarded as the origin of etched pit formation. These images also show that pit edges are preferentially oriented at 45°, 90° and 135° angles with respect to the step direction.

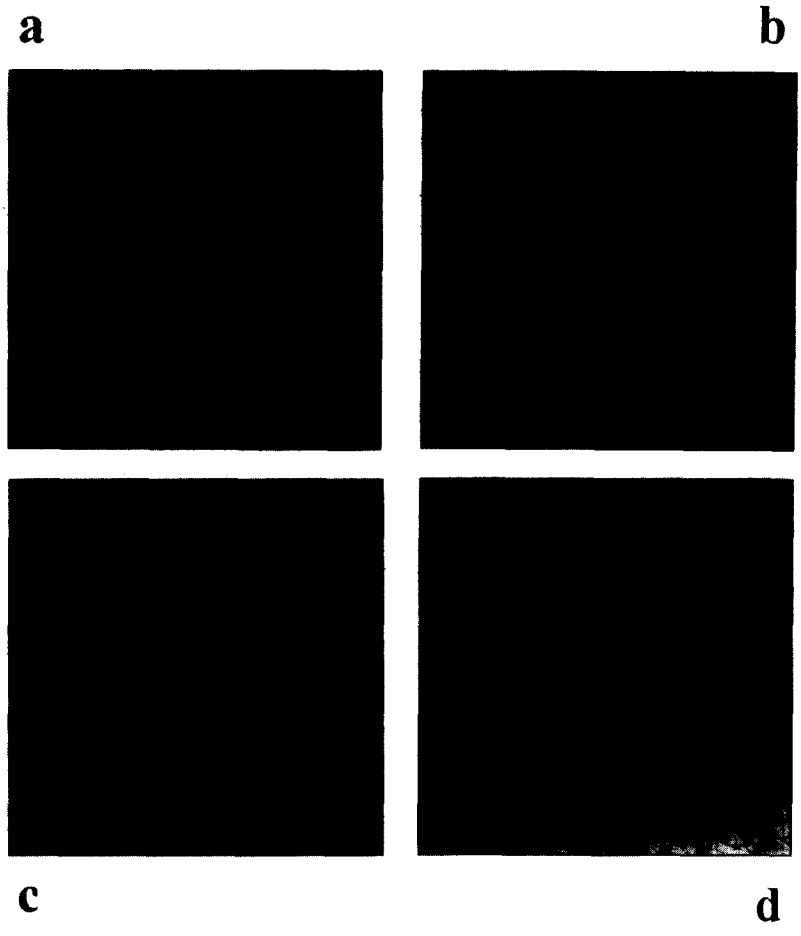

Fig. 8. *Ex situ* SFM (50000 × 50000 nm^2) of Cu surface electrodes. (a) Blank. (b) After a 30 min immersion in aqueous 1 M $HClO_4$ at $j = 6$ $\mu A\ cm^{-2}$. (c) After a 30 min immersion in aqueous 1 M $HClO_4$ + 10^{-3} at $j = 6$ $\mu A\ cm^{-2}$. (d) After a 30 min immersion in aqueous 1 M $HClO_4$ + 10^{-2} HCl M at $j = 6$ $\mu A\ cm^{-2}$.

Ex situ SFM images (50000 × 50000 nm^2 resulting from experiments made for Cu immersed in aqueous 1 M $HClO_4$ + 10^{-3} M HCl (Fig. 8(c)) reveal pit formation in agreement with results reported above in the absence of HCl (Fig. 8(b)). On the other hand, for Cu immersed in 1 M $HClO_4$ + 10^{-2} M HCl, *ex situ* SFM imaging reveals that Cu electrodissolution is accompanied by the precipitation of Cu_2Cl_2 at the interface (Fig. 8(d)). Certainly, the absence of salt formation from *in situ* STM imaging poses in this case question whether there is a tip effect when a solid salt layer is formed as tip scanning might produce either a decrease of supersaturation or the removal of the salt layer from the scanned area.

The treatment of experimental data presented in this paper constitutes the basis of further research aiming to understand the mechanism of Cu electrodissolution dynamics in different media in terms of fundamental physico-chemical phenomena. For this purpose real imaging techniques combined with surface analysis and conventional electrochemical techniques are very promising.

4. CONCLUSIONS

1. Cu specimens immersed in acids (aqueous 1 M $HClO_4$ and 0.5 M H_2SO_4) at 298 K exhibit a remarkable surface mobility at null current. The average value of the surface diffusion coefficient resulting from sequential *in situ* STM imaging is $D \cong 10^{-15}\ cm^2\ s^{-1}$. This figure is of the same order of magnitude as those of Ag atoms on Ag [13] and Au atoms on Au in acid solutions [26].
2. At a low electrodissolution rate ($j = 6$ $\mu A\ cm^{-2}$), for both acids the surface attack is considerably inhomogeneous leading to a mobile Cu interface under an unstable regime due to etched pit formation nucleated at defective sites of the Cu surface.
3. Results obtained at $j > 0$ in both acids emphasize the capability of nanoscopic techniques for evaluating local corrosion rates and the possibility envisaging for the first time etched pit initiation.
4. Comparable average rates of pit penetration (0.2 atom s^{-1}) are obtained both acid solutions.

5. The addition of HCl to both acids at concentrations lower than 10^{-3} M had no noticeable influence on the Cu electrodissolution pattern. Conversely, for concentrations higher than 10^{-2} M, the formation of a Cu_2Cl_2 layer, is detected by *ex situ* SFM imaging.
6. The absence of the salt layer produced for HCl concentration exceeding 10^{-3} M during *in situ* STM imaging poses a question about the influence of the tip to change the local conditions by either decreasing the supersaturation or removing the poorly conductive salt from the scanned area.

ACKNOWLEDGEMENTS

This work was financially supported by the Consejo Nacional de Investigaciones Científicas y Técnicas of Argentina (CONICET) and the Third World Academy of Sciences (TWAS) Associate Membership Scheme at Centres of Excellence in the South.

REFERENCES

1. B. J. Cruickshank, A. A. Gewirth, R. Rynders and R. C. Alkire, *J. Electrochem. Soc.* **139,** 2829 (1992).
2. A. A. Gewirth and H. Siegenthaler, eds, *Nanoscale Probes of the Solid/Liquid Interface*, Kluwer Academic Publishers, Dordrecht (1995).
3. T. Z. Fahidy and Z. H. Gu, *Modern Aspects of Electrochemistry* (Edited by R. E. White, J. O'M. Bockris and B. E. Conway), Vol. 27, Plenum Press, New York (1995).
4. P. Allongue, V. Kieling and H. Gerischer, *J. Electrochem. Soc.* **140,** 1008 (1993).
5. P. Allongue, V. Kieling and H. Gerischer, *J. Electrochem. Soc.* **140,** 1019 (1993).
6. J. Morales, P. Esparza, S. González, L. Vázquez, R. C. Salvarezza and A. J. Arvia, *Langmuir* **12,** 500 (1996).
7. Z. H. Gu, S. J. Xia and T. Z. Fahidy, *Electrochim. Acta* **41,** 2837 (1996).
8. G. Daccord, in *The Fractal Approach to the Heterogeneous Chemistry*, (Edited by D. Avnir), p. 183, J Wiley & Sons, New York (1989).
9. M. G. Fernandes, R. M. Latanision and P. C. Searson, *Phys. Rev. B* **47,** 11749 (1993).
10. C. S. Kohli and A. W. Ives, *J. Cryst. Growth* **16,** 123 (1972).
11. K. W. Cheng and A. W. Coller, *J. Cryst. Growth* **84,** 436 (1987).
12. K. Sieradzki, R. R. Corderman, K. Shukla and R. C. Newman, *Phil. Mag. A* **4,** 713 (1989).
13. M. E. Vela, G. Andreasen, R. C. Salvarezza, A. Hernández Cruez and A. J. Arvia, *Phys. Rev. B* **53,** 10217 (1996).
14. H. S. O. Chan, P. K. H. Ho, L. Zhuo, N. Luo, S. C. Ng and S. F. Y. Li, *Langmuir* **12,** 2580 (1996).
15. J. Krug and H. Spohn, in *Solids Far From Equilibrium. Growth, Morphology and Defects* (Edited by C. Godre(c)che), Cambridge University Press, Cambridge, England (1990).
16. F. Family and T. Vicsek, eds, *Dynamics of Fractals Surfaces*, World Scientific, Singapore (1991).
17. A. L. Barabási and H. Stanley, *Fractal Concepts in Surface Growth*, Cambridge University Press, New York (1995).
18. F. Family, *Physica A* **168,** 561–and references therein (1990).
19. W. H. Smyrl, in *Comprehensive Treatise of Electrochemistry* (Edited by J. O'M Bockris, B. E. Conway, E. Yeager and R. E. White), Vol. 4, p. 97, Plenum Press, New York (1981).
20. N. Sato and G. Okamoto, in *Comprehensive Treatise of Electrochemistry* (Edited by J. O'M Bockris, B. E. Conway, E. Yeager and R. E. White), Vol. 4, p. 193, Plenum Press, New York (1981).
21. A. Hernández Creus, P. Carro, R. C. Salvarezza and A. J. Arvia, *J. Electrochem. Soc.* **142,** 3806 (1995).
22. L. Vázquez, R. C. Salvarezza, P. Herrasti, P. Ocón, J. M. Vara and A. J. Arvia, *Appl. Surf. Sci.* **70–71,** 413 (1993).
23. J. Krim, I. Heyvaert, C. Van Haesendonck and Y. Bruyseraede, *Phys. Rev. Lett.* **70,** 57 (1993).
24. U. Bertocci and D. R. Turner, in *Enciclopedia of the Electrochemistry of the Elements* (Edited by A. J. Bard), Vol. 2, p. 383, Marcel Dekker, New York (1974).
25. C. I. Elsner, R. C. Salvarezza and A. J. Arvia, *Electrochim. Acta* **33,** 1735 (1988).
26. N. Ikemiya, M. Nishide and S. Hara, *Surf. Sci.* **340,** L965 (1995).
27. D. R. Lide, ed., *Handbook of Chemistry and Physics*, 73rd edition. CRC Press Inc USA (1993).
28. D. W. Suggs and A. J. Bard, *J. Am. Chem. Soc.* **116,** 10725 (1994).